Review of Scanning Probe Microscopy Techniques

Tim Stadelmann*

1 Introduction

1.1 About this Document

The present review has originated as an expanded version of chapter 2 of my DPhil thesis [1]. It is provided in the hope that it may serve as a useful introduction to the subject.

While I have stressed the common features of all scanning probe microscopes (SPMs) wherever possible, the focus is on the atomic force microscope (AFM) and, to a lesser degree, on the scanning tunneling microscope (STM). I have also taken the opportunity to round off the account by briefly covering topics such as the near field scanning optical microscope (NFSOM, Sec. 2.3) and the question of atomic resolution in STMs and AFMs (Secs. 2.1 and 4.6).

1.2 A Simple Idea

The fundamental principle of all scanning probe microscopes is the use of the interaction between a sharp tip and the surface of a sample to measure its *local* physical properties. Fig. 1 provides a schematic view of the interactions between the fundamental components of a generalized SPM. A map of the specimen is build by sweeping the tip across its surface scan line by scan line with a two-dimensional actuator or scanner (*cf.* Sec. 3). The scanner should ideally be able to control the relative position of the scanner to within the resolution limit imposed by the interaction; for atomic resolution this implies a precision of 1 Å or better. During this scanning process, the tip–sample interaction can be recorded directly, or, more commonly, a feedback loop keeps one parameter at a set point by varying the tip–sample distance. The correction to the distance is then used to form an image; at the same time, other surface properties can be measured.

In addition to the scanner, an SPM typically requires a mechanism for coarse positioning to bring the sample within the range of movement provided by the scanner, and to move the probe to different areas of the sample [2]. The accuracy of the positioner must be high enough to overlap the range of motion of the scanner—typically this translates to a resolution better than 1 µm in the z-direction, and several µm in the x, y-plane. The required range of movement depends on the size of the instrument and the sample and may vary from several mm to several cm. On the timescale of the measurement, the stability of the positioner must generally be within the ultimate resolution of the instrument.[1]

1.3 The Development of the Scanning Probe Microscope

1.3.1 The Stylus Profilometer

The idea of using a scanning probe to visualize the roughness of a surface is actually quite old. As early as 1929, SCHMALZ [3] developed an instrument that had much in common with the modern AFM: the stylus profilometer. A probe is lightly pressed

*mail@timstadelmann.de

[1] Drift in the z-direction may be corrected by the main feedback loop depending on the operating mode. Drift in the x, y-plane will lead to systematic distortion of the image. Noise may be reduced by mechanically decoupling the scanner and the sample from the coarse positioner.

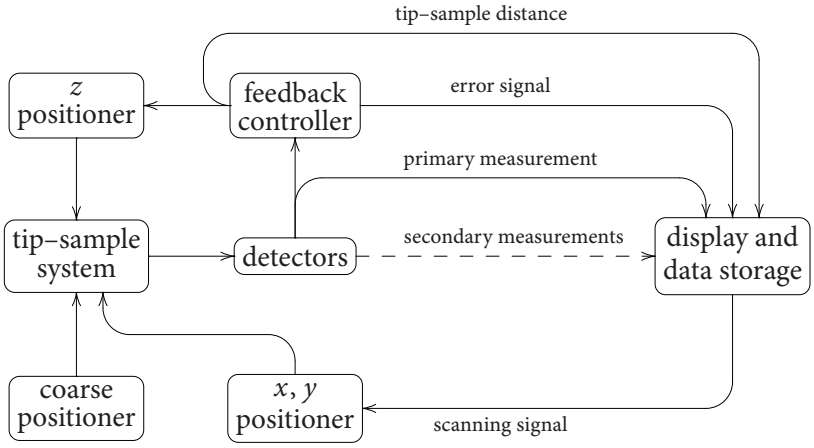

Figure 1: Schematic diagram of an SPM

against the surface by a leaf spring and moved across it; a light beam is reflected off the probe and its projection on a photographic emulsion exposes a magnified profile of the surface, using the optical lever technique (*cf.* Sec 4.3). The fundamental difference between these instruments and modern AFMs is the attainable resolution, which is limited by the relatively blunt stylus, the scanning and detection mechanism, and thermal and acoustical noise.

1.3.2 The Topographiner

The STM, which started off the development of SPMs, has its roots in the 'topographiner' advanced by YOUNG in 1971 [4, 5]. This non-contact profiler uses the current between a conducting tip and sample to sense the proximity of the surface. It already used a feedback circuit to keep the working distance constant; the use of piezoelectric positioners is another feature it shares with most modern SPMs. Unlike the STM, which places the tip close to the sample and uses direct tunneling, it operates in the Fowler-Nordheim field emission regime (*cf.* Sec 2.1). Because of this and insufficient isolation from external noise it only achieves a resolution comparable to that of optical microscopes [6].

1.3.3 Tunneling Experiments

YOUNG already used his topographiner to perform spectroscopic experiments in the direct tunneling regime and demonstrated the strong dependence of the current on the distance, but could not achieve stable imaging under these conditions [4]. Similarly, the work by GERD BINNIG and HEINRICH ROHRER, which should lead to the development of the STM, was originally centred around local spectroscopy of thin films. The idea was to use vacuum tunneling as a means to probe the surface properties [6].

1.3.4 The First Scanning Tunneling Microscope

The fundamental achievement of BINNIG and ROHRER, which was honoured with the Nobel prize in Physics in 1986,[2] was to realize that the exponential distance dependence of the tunnel current would enable true atomic resolution and to put the pieces of the puzzle together in building an microscope, the STM, that would make this vision reality [6, 7]. Unlike its predecessor, it could produce images in the direct tunneling regime and had an improved vibration-isolation system, which in the first prototype used magnetic levitation of a superconducting lead bowl [6].

1.3.5 Further Developments

Since the SPM was popularized by the work of BINNIG and ROHRER in the early 1980s, the prin-

[2] Together with ERNST RUSKA, who was awarded the other half of the prize for the invention of the electron microscope.

ciple has been applied to a wide range of problems. This includes the scanning force microscope (SFM) invented by GERD BINNIG, CALVIN QUATE, and CHRISTOPH GERBER in 1985 [8] (Sec. 4), the dynamic force microscope (DFM), which evolved as a refinement of the SFM following the work of YVES MARTIN and KUMAR WICKRAMASINGHE [9] (Sec. 4.5), and the various approaches to NFSOM [10, 11] (Sec. 2.3). The SFM in particular has become an enabling technology for several measurement (Sec. 2.2) and sample modification (Sec. 5) applications at the nanometre scale and below.

2 Applications of the SPM design

2.1 The Scanning Tunneling Microscope

2.1.1 Mechanism

The STM measures the tunnel current through the gap between a sharp tip and a conducting sample surface while the tip is scanned across the surface. Although the current can be recorded directly, it is more common to keep it constant and build an image from the z-axis correction signal [6,7,12,13]. The STM can operate in air or any non-conducting fluid, but optimal resolution may require ultra high vacuum (UHV) and low temperatures.

In the low voltage limit the tunnel current between two metal surfaces with average work function $\overline{\varphi}$ at distance z is of the form

$$I_\mathrm{t} \propto \sqrt{\overline{\varphi}} V \exp\left(-2\sqrt{2m_\mathrm{e}/\hbar^2}\sqrt{\overline{\varphi}} z\right), \qquad (1)$$

where V is the bias voltage and m_e the electron mass [4, 6, 7, 14]. As only electrons close to the Fermi energy can participate in conduction, the magnitude of the current also depends on the density of states at the Fermi level in both tip and sample.

Because of the exponential dependence on the distance, the experiment is very sensitive to variations in the topography of the sample: a step of one atomic diameter causes the tunnel current to change by 2 to 3 orders of magnitude if one assumes an average work function of order 1 eV [7]. Even more importantly, the exponential decay implies that only a few atoms at the apex of the tip significantly contribute to the current, so that the effective resolution of the instrument is much better than the sharpness of the tip suggests. It is dominated by the size of the microasperities or microtips at the front of the macroscopic tip. The macroscopic radius of curvature only matters in so far as it determines together with the surface roughness the likelihood of exactly one microtip coming within critical distance of the surface [6,7].

If the sample work function and the density of states are constant, the error signal from the feedback loop represents the topography of the sample under investigation. In practice these parameters can and will change as the tip scans across the surface, and the data is convolved with information about its electrical properties [7]. In order to correctly interpret the resulting images at atomic resolution a detailed theoretical model of the tip–sample interaction is needed [12,13,15].

2.1.2 The Tunnel Current

In the planar approximation, the exponential behaviour of the tunnel current in the low voltage limit can be understood by solving the one-dimensional Schrödinger equation for a barrier of finite height and considering the transmittivity for electrons at the Fermi level [14].[3] Eq. (1) is actually derived from SIMMONS's more general expression for the tunnel effect,

$$J_\mathrm{t} = \frac{e}{\hbar(2\pi\beta z)^2}\Big[\overline{\varphi}\mathrm{e}^{-A\sqrt{\overline{\varphi}}} - (\overline{\varphi} + eV)\,\mathrm{e}^{-A\sqrt{\overline{\varphi}-eV}}\Big], \qquad (2)$$

where J_t is the tunnel current density, $A = 2\beta z\sqrt{2m_\mathrm{e}/\hbar^2}$, and $\beta \approx 1$ for small eV [4, 16]. The approximation is valid for $eV \ll \overline{\varphi}$, while the high voltage limit corresponds to the Fowler-Nordheim field emission regime. These calculations played an important role in the initial development of the STM [6, 7], but they cannot accurately predict contrast on an atomic scale.

[3] Gasiorowicz introduces the STM in the context of cold emission. This may be misleading, as this instrument operates in the direct tunneling regime, which is precisely what differentiates it from YOUNG's topographiner.

In 1983 Tersoff and Hamann [15] introduced an approach based on first-order perturbation theory that takes into account the electronic structure of the sample; the tip is approximated by a single *s*-type wave function. It predicts a tunnel current proportional to the sample density of states at the Fermi energy evaluated at the centre of the tip orbital and is still used extensively for simulating STM images [13]. A different perturbation theory approach, which is based on the work of Bardeen, allows for a more realistic tip model and uses transfer matrices to calculate the current between the two systems. Other methods of note for calculating the tunnel current on the basis of realistic molecular models include: Scattering theory using, *e.g.*, the Landauer-Büttiker formula; the non-equilibrium Green function technique based on the Keldysh formalism, which allows for different chemical potentials in the tip and the sample and has attracted some interest in recent years [12, 13].

While these methods give realistic results for semiconductor surfaces, they severely underestimate the contrast for free-electron-like metals. Dynamic models, which take the deformation of the surface and tip crystal structures into account and consider excited electronic states, give better agreement with experiment at the expense of higher computational cost [12].

2.1.3 True Atomic Resolution

One of the main motivations behind the development of the STM is its ability to achieve true atomic resolution [6]. A measurement of a periodic structure with the correct symmetry and period may represent the envelope convolution of a complicated probe with the surface (SPMs with a blunt probe) or averaging over many layers (transmission electron microscope, TEM). It does not demonstrate the independent observation of individual atoms. Only the imaging of non-periodic structures at the atomic scale, such as defects or adatoms, allows to claim true atomic resolution. The capability of the STM in this regard was already demonstrated in 1982 by Binnig *et al.* with a prototype operating in UHV by imaging step lines on $CaIrSn_4$ and Si and fully accepted in 1985 when other groups succeeded in obtaining similar results [6].

Today, the best laboratory built STMs have a vertical resolution better than 1 pm, about 1/200 of an atomic diameter [13]. The effective resolution of the instrument is then limited by the configuration of the tip. Unfortunately, the tip geometry and composition is in general not known. While the apex shape can be determined with high accuracy by field ion microscopy [13], there is no practical way to determine the species and arrangement of the crucial atoms at the very end of the probe. Moreover, this configuration may change during normal operation as the tip is deformed and picks up atoms from the surface. In fact, it is normal practice to repeatedly bring the tip into contact with the sample until a tip configuration is created that has only one significant microtip with orbitals giving optimal contrast [13]. As a result, our understanding of the mechanisms leading to contrast at the atomic scale is still limited, and the interpretation of images is often ambiguous and may require careful comparison with simulations assuming different tips.

2.2 The Scanning Force Microscope

2.2.1 Principle

An SFM uses the deflection or resonant frequency of a cantilever or leaf spring to measure the force between a probe attached to its end—usually a sharp tip—and the sample under investigation. In analogy to the tunnel current in the STM, the force can be recorded directly or kept constant by means of a feedback loop. The operation of the SFM is discussed in more detail in Section 4.

2.2.2 The Atomic Force Microscope

The archetypal SFM is the AFM invented by Binnig, Quate, and Gerber in 1985 [8], which uses the repulsive force between a sample and a sharp tip pressed against it and measures the sample topography. Unlike the STM, it is not limited to conducting samples.

2.2.3 Other Forces and Functionalization

The operational principle of the SFM is quite general and there are many forces that can be measured. An AFM may also use the attractive force felt by a tip close to the sample surface and the lateral force that results from friction as the tip is scanned across the surface. Moreover, the tip can be functionalized so that magnetic (magnetic force microscope, MFM), electrostatic, or chemical forces can be detected. Since the SFM provides the capability of scanning a probe across a surface with great accuracy without placing many constraints on the properties of the tip or the sample it also forms the basis for other measurement and lithography[4] techniques. This includes local capacitance (scanning capacitance microscope, SCM) and conductivity measurements as well as mechanical and electrochemical sample modification methods.

2.3 The Near Field Scanning Optical Microscope

2.3.1 Conception

The NFSOM provides a way of probing the optical properties of a surface at length scales smaller than the optical wave length [10, 11, 17, 18]. It avoids the diffraction limit is by using a light source or detector whose size and distance from the sample is much less than the wave length so that the interaction is dominated by the near field. The resolution is then limited by the effective aperture size.

The idea of utilizing the near field zone of an aperture in combination with scanning to form an image with sub-wave-length resolution was already proposed by SYNGE in 1928 [18] and accomplished with microwaves by ASH *et al.* in 1972 [10, 18]. Inspired by the contemporary work on STM, POHL *et al.* built the first first working NFSOM using wave lengths in the visible range from 1982 to 1983.

[4] From Greek λίθος, 'stone', and γράφειν, 'to draw'. Originally referring to printing with a limestone, the word has come to mean any pattern transfer technique.

2.3.2 Requirements

The main challenges in realizing a NFSOM are to achieve enough brightness with a small aperture to allow for reliable detection and to bring the aperture close enough to the surface of the sample [18]. While the former has become feasible in the 1980s because of advances in laser and detector technology, the latter was made possible by placing the aperture at the apex of a sharp dielectric tip. A probe of this kind can be manufactured by etching a material such as quartz to a sharp point, covering the resulting tip with a metal layer, and opening a hole at the apex by mechanical or chemical means [10].

2.3.3 Distance Control

Various approaches can be used to control the distance between the probe and the sample. It is possible to simply let the tip touch the sample or a constant distance may be approximately maintained by controlling the tip position using capacitive or interferometric sensing [10]. However, techniques based on STM [10] or DFM [18] have proved most useful as they allow for maintaining a constant gap at the nanometre scale and allow for simultaneous measurement of the surface topography.

2.3.4 Operating Modes

Similar to conventional optical microscopes, NFSOMs can be operated either in transmission or reflection mode. Although it is possible to use the tip for both emission and detection in reflection mode, it is difficult to achieve a useful signal-to-noise ratio with this setup and generally the scanning probe is used either for illumination or measurement: In illumination mode, the tip forms the light source and the detector uses conventional optics, while in collection mode the sample is illuminated broadly and the light coupled into the probe through the aperture is measured [18].

2.3.5 The Photon Scanning Tunneling Microscope

A variant of collection mode NFSOM is the photon scanning tunneling microscope (PSTM) introduced

by Reddick in 1988 [11]. Here, an optical evanescent wave is set up at the surface of the sample by total internal reflection. If an optical probe is brought close to the surface, photons tunnel into the probe and can be detected. The field intensity outside the sample and the tunnel current decrease exponentially with increasing distance:

$$I \propto \exp\left(-2kz\sqrt{\sin\theta - (n_\mathrm{t}/n_\mathrm{i})^2}\right), \qquad (3)$$

where k is the wave number, z the distance, θ the incident angle, and n_t and n_i the refractive indices of the gap and the sample. The tunnel signal may be kept constant by a feedback loop that adjusts the distance of the tip to the sample. Operation is then analogous to that of an electron STM, providing a measurement of the surface topography convoluted with the local *optical* properties of the sample [11, 18].

2.3.6 Interpretation of Images

Similar to the situation with STM, it is difficult to formulate simple rules for contrast formation in the near field. In particular, intuitions form conventional far field optics do not carry over directly, and the behaviour depends on the properties of the sample [18]. Correct interpretation of the data requires a detailed theoretical model of the interaction between the tip and the sample surface [17].

3 The Scanner

3.1 Overview

Apart from the detection mechanism, the three-dimensional scanner is the most important component of an SPM. It must be able to control the relative position of the sample and the tip at the intended resolution of the instrument. Its capacity to respond quickly to changes in the set point and hence follow the surface topography limits the scanning rate at which the maximal resolution can be realized.

For lithography applications, the ability of the scanner to accurately return to a specific position after covering a potentially large area is essential to ensure that individual parts of large patterns can fit together.

The mechanical resonant frequencies of the scanner are also important, since they determine the acceptance of external acoustic noise and restrict the feasible scanning frequencies. To ensure that all resonances occur at high frequencies, the entire scanning assembly must be mechanically stiff.

3.2 Piezoelectric Scanners

3.2.1 Background

Most commercial and research SPMs use scanners based on piezoelectric actuators. These positioners are not affected by backlash or discrete step sizes and offer theoretically unlimited resolution. That the deformation is indeed continuous even for polycrystalline piezoceramics was ultimately only established by the original STM experiments [6]. In practice, resolution is limited by noise and the finite accuracy of the control electronics.

3.2.2 The Piezoelectric Effect

In crystalline dielectrics that lack inversion symmetry, such as quartz or tourmaline, mechanical stress along certain crystal axes causes the unit cell to become polarized as the charged atoms forming its basis move relative to each other. The direct piezoelectric[5] effect was discovered by Pierre and Jacques Curie in 1880. The polarization of the material is a linear function of the stress and in the absence of an external electrical field is given by

$$P_i = d_{ijk}\sigma_{jk}, \qquad (4)$$

where P_i is the polarization vector, σ_{jk} is the mechanical stress, d_{ijk} is called the piezoelectric strain tensor, and the Einstein summation convention has been used [19]. As a third-rank tensor, d_{ijk} has 27 components, but since the stress tensor σ_{jk} is symmetric no more than 18 of them are independent.[6]

[5] from Greek πιέζειν, 'to squeeze'

[6] In engineering texts, i and j are sometimes contracted into a single index that runs over the 6 independent components of the strain tensor. This is known as Voigt's notation.

Conversely, an external electric field changes the equilibrium configuration of the basis atoms and leads to a deformation of the crystal, which is described by another linear relation:

$$\varepsilon_{jk} = d_{ijk} E_i, \tag{5}$$

where ε_{jk} is the strain tensor, E_i is the electric field vector, and the material is assumed to be relaxed. The converse piezoelectric effect constitutes the underlying principle of piezoelectric actuators [19].

3.2.3 Ferroelectric Ceramics for Actuator Applications

Actuators are most commonly assembled from ferroelectric ceramics such as lead zirconate titanate (PZT, $Pb(Zr_xTi_{1-x})O_3$). Ferroelectric materials are piezoelectric materials that spontaneously polarize below the Curie temperature T_C because of symmetry breaking and can produce a strong piezoelectric response even as a polycrystal since the orientation of the polarization can be changed externally. The individual pieces of ceramic are produced by pressing a precursor powder in the desired shape and sintering the workpiece. The resulting actuator is polycrystalline with randomly oriented grains and polarization domains and has initially almost no ability to expand or contract. In order to polarize the ceramic, the pieces are heated above T_C and cooled down in the presence of a strong electric field. After this process, the polarization direction in the grains mostly coincides with the equivalent crystal axis that is best aligned to the external field [19].

3.2.4 Deviations from Linearity

Although the piezoelectric effect, Eq. (5)), is linear in nature, practical actuators exhibit a certain degree of nonlinearity [20–23]: For ferroelectric ceramics, the piezoelectric strain tensor depends on the average remnant polarization, which can change with time or in response to an external electric field. The effect is small for low driving voltages and small extensions and has consequently been of limited importance to atomic scale imaging, which was the initial focus of SPM. Metrology and lithography applications, however, require accurate calibration and repeatability over a large scanning area and hence are critically affected by nonlinearity and drift [20, 21].

As the strength of the piezoelectric response is affected by the external electric field, the strain depends on the speed and direction of the change in the driving voltage. Accordingly, the relation between input voltage and displacement exhibits hysteresis. In typical ferroelectric actuators the error caused by hysteresis is 5 % to 10 % of the extension [22].

Even in a constant electric field the extension of the ferroelectric material initially continues to change slowly, an effect which is known as 'creep' or 'drift'. It is caused by the movement of the walls between individual polarization domains, which results in a change of the average polarization.

Over the lifetime of an actuator the alignment created by the poling process may degrade. This is especially true if the piezoceramic is heated to temperatures close to T_C, exposed to high electric fields in the direction opposite to its polarization, or used only rarely. Conversely, regular use of the actuator prevents degradation and can actually improve the alignment.

3.2.5 Error Correction Strategies

A piezoelectric actuator in general and an SPM scanner in particular may be operated either in open or closed loop configuration. In open loop mode a mathematical model or a set of calibration data is used to derive the required driving signal from the desired position, while in closed loop mode the actual position of the scanner is measured and used as the input of a feedback loop.

In the open loop configuration, the software can correct for deviations either by processing the finished image (off-line) or by modifying the driving signal of the scanner (on-line). On-line operation ensures uniform resolution over the entire scanning area. Software using a sophisticated theoretical model of the scanner can compensate for most of the nonlinearity and hysteresis, but does not correct for drift and aging [22, 24]. Performance depends on the the accuracy of the model and the repeatability of the physical scanner behaviour.

Closed loop operation requires an accurate measurement of the scanner position. This is routinely achieved using capacitive [20, 22, 24, 25] or interferometric [23, 25] sensors. In this mode, performance is generally determined by the accuracy of the sensors [23] and the response time and stability of the feedback loop. An increasing number of SPMs use hardware feedback since it allows the scanner to return to a precise point on the surface, a property that is particularly important for lithography and metrology applications.

The hysteresis of a piezoelectric positioner can also be reduced by using the charge instead of the voltage as the controlling parameter [21, 25]. This approach may be combined with other error compensation strategies, but reduces the effective resolution of the actuator [24].

For scanner designs that do not rely on the linearity of the piezoelectric effect, which changes its sign if the electric field is reversed, electrostrictive[7] materials are a viable alternative [25]. Electrostriction is a property of all dielectrics, which deform in proportion to the square of the external electric field. Because of its strong electrostrictive response, the material most widely used for actuators is lead magnesium niobate (PMN, $Pb(Mg_{1/3}Nb_{2/3})O_3$) [19]. PMN exhibits less creep and hysteresis than PZT, but has a stronger temperature dependence and smaller range for similarly sized actuators. In practice, its use in SPM scanners is limited to applications where control of the hysteresis is crucial, such as force-distance measurements [25].

3.2.6 Basic Actuators

In the presence of an external electric field parallel to its average polarization, a rod of ferroelectric material will expand along the polarization axis and contract normal to it, as shown in Fig. 2(a). If the electric field is reversed, the rod will contract along the poling axis and expand in the perpendicular direction. A rod of this kind can be used as a simple one-dimensional actuator, the range of which is proportional to its length and the range of the electric field. The field strength in the poling direction is limited by dielectric breakdown, while the allowable field strength in the inverse direction is typically much lower and given by the onset of depoling. The field required to achieve the theoretical maximal extension of a rod of commercially available PZT is several kV/mm, which makes this design impractical for many applications. Instead, the arrangement shown in Fig. 2(b) is commonly used. Here the rod is replaced by a stack of thin piezoelectric disks with alternating poling connected in parallel. The voltage required to reach full extension is divided by the number of disks.

The deformation normal to the direction of the electric field can also be exploited in piezoelectric actuators. In Fig. 2(c) two layers of ferroelectric material are combined in an arrangement similar to a bimetallic strip. Application of an external voltage causes one of the layers to expand while the other contracts so that the device bends upwards. If one end is clamped, the other will move in an arc by a distance much larger than the deformation of the ceramic. In general, a stacked structure comprising an arbitrary number of piezoelectric and elastic layers is known as a multimorph, which makes the structure in Fig. 2(c) a bimorph. A familiar application of this idea—frequently used as a transducer or loudspeaker—is the unimorph[8] disk shown in Fig. 2(d) consisting of just one piezoelectric layer attached to an elastic metal base, which doubles as one of the contacts. If a voltage is applied, the disk buckles axially.

3.2.7 Scanner Design

Tripod Fig. 3(a) shows the most straightforward three-dimensional scanner geometry, which was used by BINNIG *et al.* [7] in the earliest SPM experiments. A separate one-dimensional piezoelectric actuator—typically a standard PZT stack—is used for each axis of movement. Since the position on the individual axes can be controlled independently, the feedback and data acquisition modules can be kept simple. Even so, because of the geomet-

[7] From Latin stringere, 'to draw tight'

[8] Rather confusingly, the similar term 'monomorph' is sometimes used to describe a different actuator lacking the elastic layer. Buckling is then induced by an inhomogeneous field.

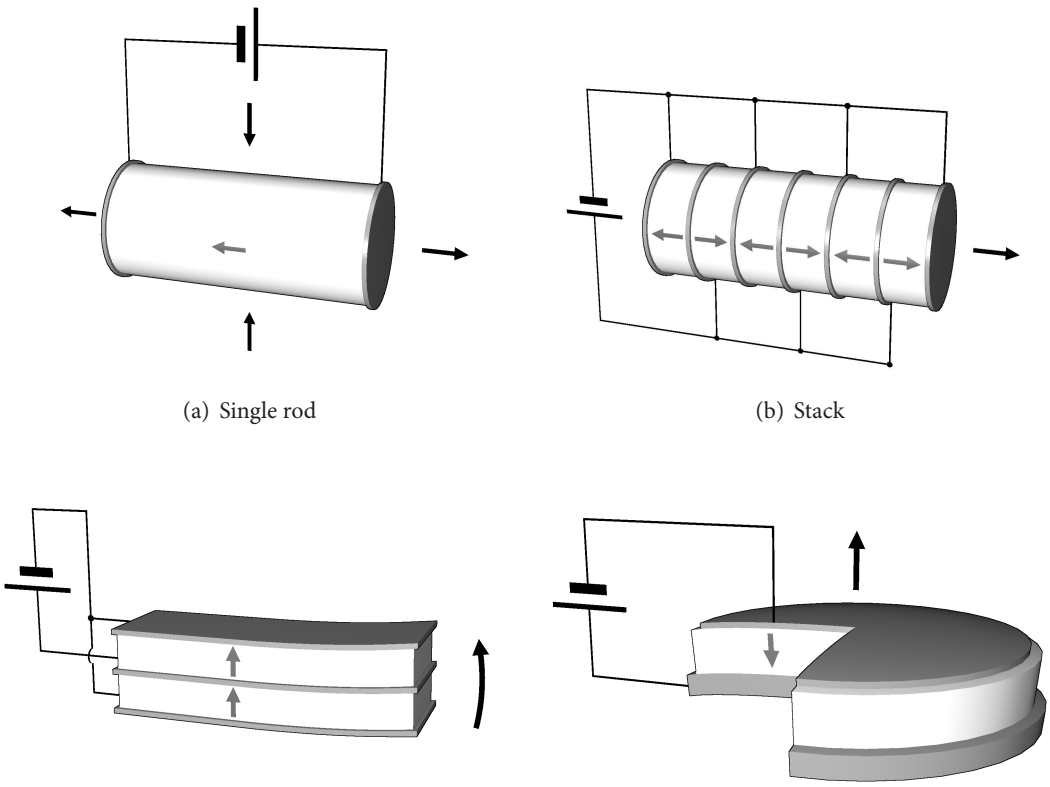

(a) Single rod (b) Stack

(c) Bimorph (d) Unimorph disk

Figure 2: Basic piezoelectric actuators made from ferroelectric ceramic. Grey arrows indicate average polarization. Black arrows show deformation or movement.

rical coupling of the actuators cross talk of the order 0·1 % to 1 % between the axis is present and may need to be corrected for [26]. The disadvantage of this design is an increased mechanical complexity and a limited range of movement in the plane of the sample.

Single Hollow Tube In 1986 Binnig *et al.* introduced a sophisticated scanner, which requires only one piece of piezoelectric material [27, 28]. The design makes use of the transverse component of the piezoelectric response and is now used in the majority of new SPMs. As illustrated in Fig. 3(b), the piezoceramic is formed as a hollow tube with a single contact on the inside as well as four contacts on the outer surface, where each covers a quarter of the circumference. By applying equal and opposite voltages V_x (V_y) to opposing quadrants of the tube, the sides are induced to contract and expand respectively, and the tube bends. At the same time, a bias voltage V_z applied to all four quadrants with respect to the central contact changes the length of the entire tube. If one end of the tube is clamped to the support of the instrument, the other end, which may hold either the sample or the probe, can scan a three-dimensional volume [2, 27]. The range of sideways movement that can be achieved in this manner is much larger than the longitudinal expansion of the sides of the hollow tube. The drawback is that the movement in the (x, y)-plane and along the z-axis is no longer independent. The interference between the three axis is much larger

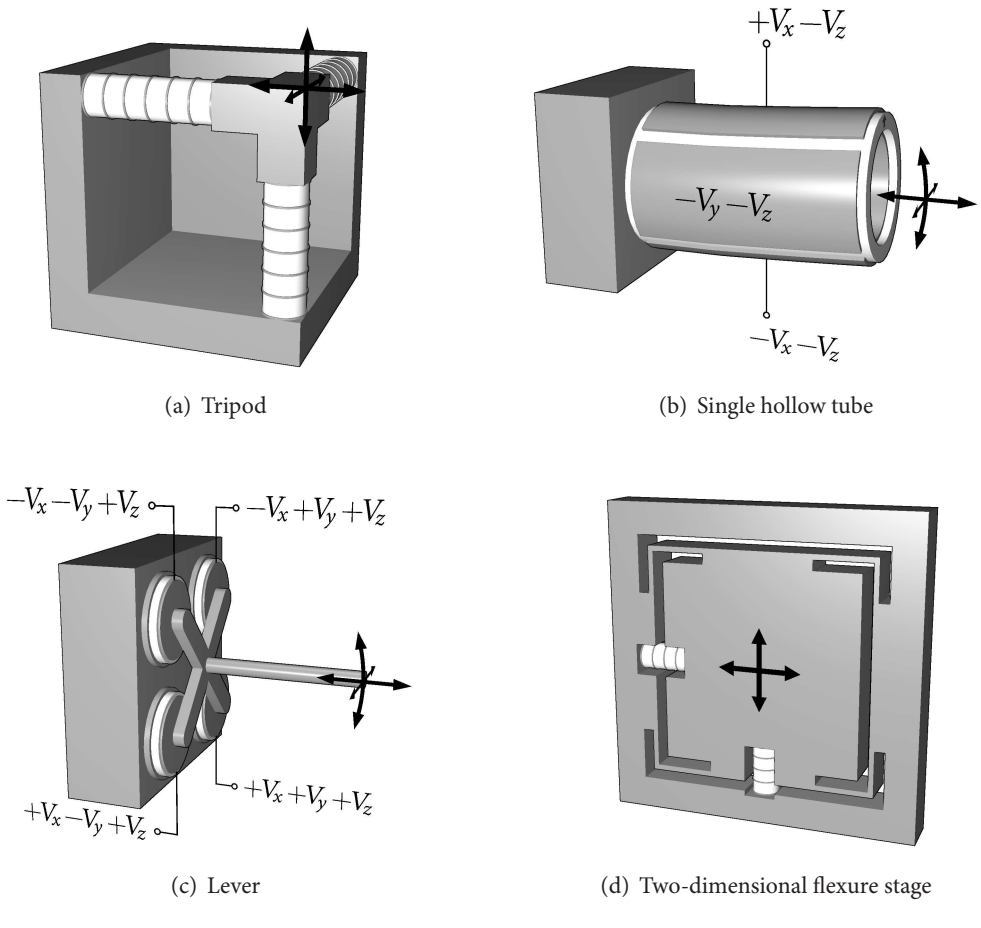

(a) Tripod

(b) Single hollow tube

(c) Lever

(d) Two-dimensional flexure stage

Figure 3: Piezoelectric SPM scanners. Arrows indicate scanner movement.

than with the tripod geometry: The free end of the tube maps out a curved surface if V_z is kept constant. Moreover, a complex controller module is required to translate (x, y, z)-values into voltages.

Lever Design Fig. 3(c) shows a design proposed by MARIANI *et al.* [29] that is conceptually similar to the tube scanner but does not require a specialized piece of piezoceramic. Instead, four standard unimorph disk actuators are laid out in the corners of a square and connected by a rigid cross supporting a lever. If the actuators on one side of the square retract while the ones on the other side move upwards the lever swings to that side. Movement along the lever axis—with a limited range given by the travel of the disks—can be achieved by driving all four actuators in parallel. The design suffers from the same cross talk problems as the tube scanner and a lessened stiffness, but can be implemented very cheaply and allows for potentially very large backlash-free amplification of the movement in the (x, y)-plane (at the expense of reduced stiffness) [29]. A further simplification uses a single disk divided into four quadrants instead of four separate actuators.

Flexure Stages Conventional three-dimensional scanners are not only afflicted by cross talk, but take up space directly above or below the point where the probe comes in contact with the sample, making it difficult to integrate the SPM with other microscopy techniques. This is particularly problematic for near field optical microscopy. Several schemes have been proposed to move the scanner hardware away from the optical axis and contain it in a flat package [30]. A design that uses a set of

leaf springs and levers to transmits the movement of an off-axis actuator to the sample stage as illustrated in Fig 3(d) has proven particularly useful. The entire device is machined from a single piece of metal, and hinges are provided by the flexure of thin metal bridges, avoiding backlash and the need for lubrication [23, 31]. Geometrical amplification of the movement range is possible by a suitable arrangement of levers as in the original design by Scire [31], but reduces the stiffness of the translator [26]. It is possible to combine several independent stages, although the combination of x and y scanners in a single frame as shown in Fig. 3(d) helps minimizing Abbe errors [31].

3.3 Electromagnetic Scanners

3.3.1 Electrodynamic Actuators

In an electrodynamic or inductive actuator a solenoid carrying the driving current moves in the radial field between the poles of a permanent magnet. The solenoid experiences a force, which is balanced by a diaphragm or spring, so that the displacement of the actuator is

$$d = \frac{F}{k} = \frac{nI\Phi}{k}, \tag{6}$$

where F is the force, k the spring constant, n the number of windings in the solenoid, I the current, and Φ the magnetic flux in the gap.

This arrangement, often know as a voice coil, is familiar from acoustic loudspeakers and used to see widespread use in the laboratory for micropositioning applications. Despite the fact that electrodynamic actuators are virtually free from hysteresis and drift and do not require high voltage electronics, they have been superseded by piezoelectric elements for fine positioning [32]. In conventional voice coil designs a moderate current causes a large displacement and the device has a low resonant frequency. Nanometre resolution would require a sensitive current control that is impossible to achieve in practice and the actuator position is highly susceptible to acoustic and electromagnetic noise on this length scale.

Binnig *et al.* [33] have shown that these disadvantages may be overcome by increasing the spring constant that the solenoid pushes against to such an extent that the travel for conveniently controllable driving currents is reduced to the desired scanner range. The deviations caused by instabilities in the driving current are demagnified proportionally so that the need for sensitive electronic control is obviated. At the same time, the effective stiffness of the scanner is increased, leading to higher mechanical resonance frequencies and reducing the interference from the scanning frequency and low frequency acoustic noise.

3.3.2 Scanner Design

Electrodynamic actuators can be used to construct a three-dimensional scanner in much the same way as piezoelectric actuators. While there is no analogy to the the hollow tube design of Fig. 3(b), the other scanners shown in Fig. 3, which use individual one-dimensional positioners, can be implemented readily. Most commercial offerings use a form of flexure stage, while Mariani has realized a variant of his inexpensive lever scheme that employs standard voice coils [32]. Binnig *et al.* [33] have used a central lever that doubles as the elastic load for both x and y actuators.

Unlike piezoelectric scanners, electromagnetic devices can deliver large travel ranges even with small actuator sizes. This makes them the preferred solution for applications where miniaturization is important, for example where a large number of probes is to be operated independently within a limited area [34].

4 A Closer Look at Scanning Force Microscopy

4.1 Overview

In this section I shall explain the operation of scanning force microscopes in more detail. Naturally, special attention is given to the atomic force microscope, and the various ways of functionalizing the tip of an sfm or using it as an enabling technology for other microscopy methods are not covered.

sfms use the deflection or resonant frequency of a cantilever as a measure of the tip–sample interaction. The deflection of the probe must be measured

with sufficient accuracy to achieve the desired resolution, and Sec. 4.3 compares various approaches to this problem. The dynamic force microscope expounded in Sec. 4.5 vibrates its probe, and the frequency response is determined; otherwise, the interaction force is recorded directly in a static force measurement.

In Sec. 4.6 I shall briefly touch on the capability of AFM for atomic resolution imaging. Finally, in Sec. 4.8 the origins of artefacts in AFM images are discussed.

4.2 The Probe

As shown in Fig. 4, an SFM probe consists of a sensing tip attached to the end of a flexible cantilever. Nowadays, a large range of probes for different applications is commercially available. The tip is characterized by its shape as well as its electrical, chemical, and mechanical properties. It is manufactured from a crystalline material by mechanical crushing, or, more commonly, chemical etching. The tip angle determines the ability of the probe to follow rough surfaces exhibiting features with high aspect ratios. The tip radius limits the resolution of measurements using long-range forces. Silicon tips with tip angles of approximately 10° and radii of curvature of 20 nm are readily available. Even sharper tips are possible for specialized applications. For electrochemical applications, electronic measurements, and DFM measurements in the presence of a bias voltage, tips must be conducting. This often means heavily doped semiconductors or metal coatings, but for conduction measurements solid metal tips may be required. For mechanical surface modification, diamond tips can be used.

The elastic deformation of the cantilever bearing the tip is used to measure the tip–sample interaction. The deflection z is approximately proportional to the applied force F_{ts}:

$$F_{\mathrm{ts}} = kz, \tag{7}$$

where k is the stiffness of the cantilever. For a rectangular beam,

$$k = \frac{Et^3 w}{4(\ell - \Delta\ell)^3}, \tag{8}$$

where E is Young's modulus and $\Delta\ell$ the distance of the tip from the end of the cantilever. In practice, a V-shaped cantilever is often used in an attempt to increase the lateral and torsional stiffness, although SADER [35] has shown that this line of reasoning is in fact incorrect and V-shaped cantilevers are *more* susceptible to lateral forces. For such a cantilever,

$$k = \frac{Et^3 w}{2(\ell - \Delta\ell)^3}\left(1 + \frac{4w^3}{b^3}\right)^{-1}. \tag{9}$$

The stiffness of the cantilever determines the sensitivity and the resonant frequency. According to Hooke's law (7), a stiffer cantilever deflects less for the same force, and therefore has a larger range and reduced sensitivity. The force that can be measured in the repulsive regime is limited by the sample's threshold for inelastic deformation. For typical AFM applications, a cantilever is chosen that is compliant enough to allow for easy detection of forces significantly below this limit. The movement of the cantilever in air or vacuum can be approximated by that of a point mass on a massless spring; the resonant frequency is then

$$\omega_0 = \sqrt{\frac{k}{m^*}}, \tag{10}$$

where m^* is the effective mass. This frequency governs the susceptibility of the cantilever to external noise and dictates the approximate frequency at which it must be vibrated in a DFM.

4.3 Detection Strategies

4.3.1 Tunneling Probe

The original atomic force microscope proposed by BINNIG, QUATE, and GERBER [8] uses the tip of an STM to measure the deflection of a conducting cantilever bearing the AFM tip as shown in Fig. 5(a). This method can use separate feedback loops for the AFM and STM parts of the experiment. Because of its complexity, limitation to conducting cantilevers, and sensitivity to contamination it is of little relevance nowadays.

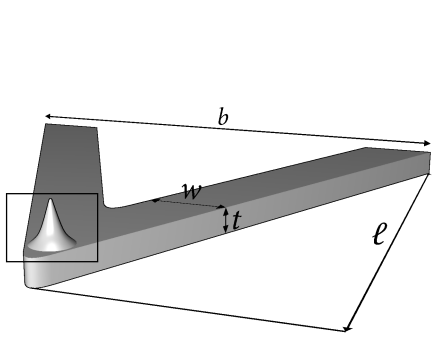

(a) V-shaped cantilever with width w, length ℓ, and thickness t

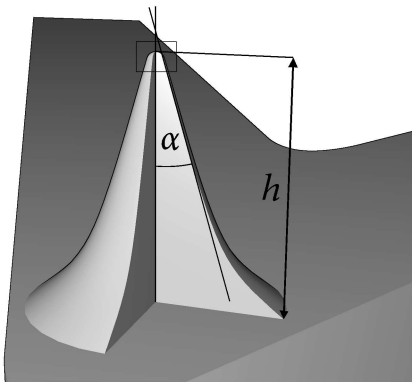

(b) Tip with height h and angle α

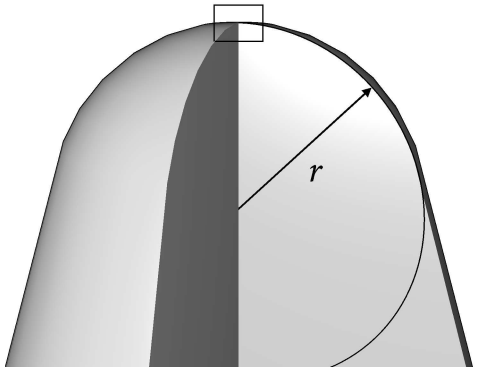

(c) Apex with radius of curvature r

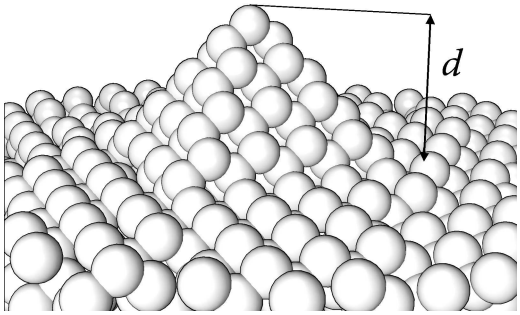

(d) Microtip with height d

Figure 4: An atomic force microscopy probe at different magnifications. The thin box shows the location of the image at the next magnification step.

4.3.2 Interferometer

The interferometer is a standard instrument for measuring small changes in position: Light is sent along two different paths, one of which depends on the displacement to be measured. The light is then allowed to interfere, and the relative phase, which depends on the path difference, can be determined. The technique can be applied straightforwardly to the SFM as shown in Fig. 5(b) and has the advantage of providing an intrinsic calibration of the deflection via the wave length [9, 36].

4.3.3 Optical Lever

Today, most SFMs use the inexpensive optical lever technique illustrated in Fig. 5(c) to measure cantilever deflection. A collimated beam of light is reflected off the cantilever and projected on a position-sensitive photodetector (PSD). A detector with two segments allows the detection of the movement along one axis only, while one with four segments will detect a shift along the perpendicular direction as well. The bending of the cantilever changes the angle of incidence, so that the deflected beam falls onto a different vertical position on the PSD; a lateral shift is caused by torsion in the presence of a frictional force. In both cases the shift of the spot depends on the distance between the cantilever and the PSD; given sufficient stability, even small tilts can be detected easily [37].

This method was known long before the SFM existed, being used in early profilometers which are conceptually similar to AFMs but operate at much lower resolution. Instead of a PSD, these instru-

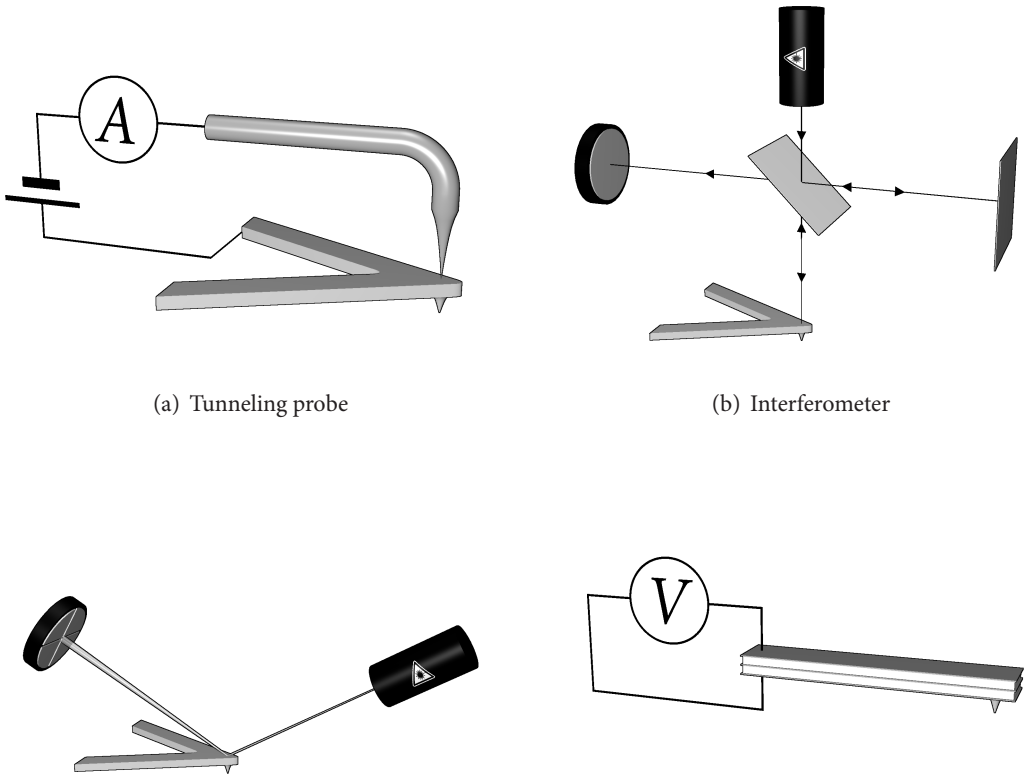

(a) Tunneling probe

(b) Interferometer

(c) Optical lever

(d) Piezoelectric cantilever

Figure 5: Detection strategies for SFM cantilever deflection

ments used a moving strip of photographic film, on which a magnified representation of the sample profile would be traced by the reflected beam.

4.3.4 Piezoelectric Cantilever

Fig. 5(d) shows how the deflection can be measured directly by using a cantilever built from a piezoelectric unimorph or bimorph sensor (see Section 3.2.6). As no external detection mechanism is required, the complexity of the instrument is reduced. However, fabricating and changing the cantilevers is more difficult and expensive. Piezoelectric detection is particularly interesting for applications where an external detection mechanism is difficult to implement because of limited space or accessibility [38, 39].

4.4 Tip–Sample Interaction in the Atomic Force Microscope

4.4.1 The Problem

In contrast to the STM, there is in general no useful approximation such as Eq. (1) for the force between the tip of an AFM and the sample. Instead, the potential has contributions from different interactions. Some of these contributions decay more slowly than the tunnel current, so that the macroscopic shape of the tip and the medium play an important role and a purely local model may be insufficient to predict the force on the tip. Even so, short-rage forces between the atoms at the tip apex and the sample may still enable atomic resolution. Especially when operating in the repulsive regime, the interaction force can be high enough that the elastic deformation of the tip and the sample

must also be taken into account [25]. For topographic measurements at the scale of several nanometres and above, these complications can often be ignored, but understanding contrast at the atomic scale and between different materials depends on a realistic model of these forces.

4.4.2 Interaction Regimes and Jump-to-Contact

In general, the potential has a strongly repulsive part at small distances, which ultimately results from the Pauli exclusion principle, and an attractive part at larger distances, which results from the exchange and electromagnetic interactions. Fig. 6(a) uses the familiar Lennard-Jones potential to illustrate this point. It should, however, be noted here that the Lennard-Jones potential, while it captures the essential features of most realistic potentials, is *not* generally a good model for the tip–sample interaction.

Fig. 6(b) shows the interaction force corresponding to the potential in Fig. 6(a). The cantilever holding the tip above the sample deforms until the elastic force $F_c = k(d - z)$, where k is the stiffness of the cantilever and z its position above the sample, exactly balances the tip–sample interaction force F_{ts}. If the stiffness k is smaller than the largest slope along the curve F_{ts}, there is a region in the attractive part of the potential where two stable equilibrium deflections $d-z$ correspond to a single cantilever position z. The straight lines in Fig. 6(b) correspond to the elastic force of a cantilever at the two positions $z = a$ and $z = b$ delimiting this range; the two points where the forces balance are marked α (β) and α' (β'); for cantilever positions between a and b, there is a third (metastable) point where $F_c = F_{ts}$. When the probe approaches the surface, the deflection increases continuously until it reaches a, where the deflection increases suddenly and the tip jumps from the position corresponding to α' to that corresponding to α. During retraction the deflection changes continuously until the cantilever reaches b, where the tip jumps from β to β'. Consequently, the interaction force measured as a function of the cantilever position z shows discontinuities and hysteresis; the part of the force-distance curve between α' and β is never sampled. The two discontinuities are known as 'jump-to-contact' and 'jump-off-contact', respectively. They can only be avoided by increasing k, which leads to smaller deflections and a lower signal-to-noise ratio [25, 38].

4.4.3 Important Contributions to the Tip–Sample Interaction

Under ambient conditions, many surfaces including oxidized semiconductor surfaces are covered by a thin layer of adsorbed water [25, 36]. Once the water layers on the tip and the surface touch, a meniscus is formed and the surface tension pulls the tip towards the sample. The influence of the water layer is small before the meniscus forms, but once it has formed, it dominates the interaction, extending far from the sample as the meniscus is stretched. The magnitude of the meniscus force is a complicated function of the distance and depends on the shape of the tip; for large $d \gg r$ it varies approximately as $1/d$ until the meniscus ruptures [25].

At large distances and in the absence of a meniscus force, the interaction is dominated by the van der Waals force. This force results from electromagnetic dipole interactions. Between individual atoms or molecules, all contributions to the van der Waals force vary as $1/d^7$. It is generally attractive, but can become repulsive in dense media. The situation is more complicated for macroscopic bodies. Assuming isotropy and additivity, the force between a surface and a sphere of radius r at a distance $d \ll r$ is approximately proportional to d/r^2 [25, 40].

If there is a voltage difference between the tip and the sample, an attractive Coulomb force pulls them together. For a tip with radius of curvature r, the force varies with distance as $1/d$ if $r \gg d$ and as $1/d^2$ if $r \ll d$ [25]. If the tip or the sample are conducting, image forces have to be considered as well. For topographic measurements at the nanometre scale and above, the force caused by an intentional bias can be used to improve the stability of a dynamic force microscope [36].

Chemical forces result from the interaction of the electron clouds and nuclei at the apex of the tip

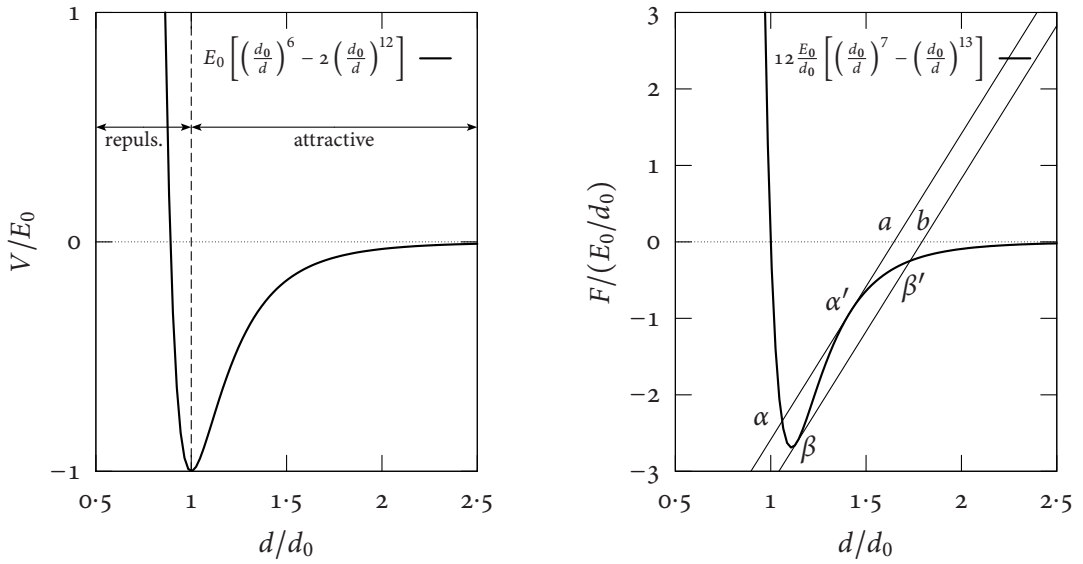

(a) Example potential with attractive and repulsive parts

(b) Interaction force corresponding to the potential in (a). Straight lines represent the elastic force of the cantilever.

Figure 6: Features of the tip–sample interaction in an AFM.

with those at the sample surface. They are the same forces that are responsible for covalent and hydrogen bonds and cause the repulsion that is measured in contact AFM. The attractive part of the potential decays very rapidly with distance, and it is this behaviour that enables atomic resolution in an AFM, since it means that only the microtip coming closest to the sample contributes significantly to the interaction [12, 13].

4.5 Dynamic Force Microscopy

4.5.1 Mechanism

A DFM is an SFM in which the cantilever and tip system is vibrated close to a resonant frequency, usually using a piezoelectric transducer. The dynamic behaviour of the cantilever changes as a result of the tip–sample interaction, and it is this change that is measured and used to form an image. The original AFM by BINNIG *et al.* already included dynamic force capabilities [8], but static force measurements were found to be more reliable. The first working DFM was demonstrated by MARTIN *et al.* [9] in 1987. Compared to static force microscopy, DFM is more suitable for measurements in the attractive region of the tip–sample potential and avoids jump-to-contact. The signal-to-noise ratio can be improved by using narrow-band detection in combination with a standard lock-in technique [38].

4.5.2 The Frequency Shift

The motion of the cantilever can be approximated[9] by that of a point mass on a massless harmonic spring [12, 40, 41]. In the presence of a tip–sample interaction force $F_{\text{int}}(z)$ and a driving force $F_{\text{ext}}(t) = F_0 \cos(\omega t)$ the equation of motion is

$$m^* \ddot{z} + 2\gamma m^* \dot{z} + k\,(z - z_0) = F_{\text{ts}}(z) + F_{\text{ext}}(t), \quad (11)$$

where m^* is the effective mass, γ the damping coefficient, and k the stiffness. If the amplitude of the oscillation is small compared to the distance over which $F_{\text{ts}}(z)$ changes, $F_{\text{ts}}(z) \approx (z - z_0)F'_{\text{ts}}(z_0)$. For realistic long range interaction forces, this approximation is valid if the amplitude A is much

[9] This is a reasonable approximation for cantilevers *in vacuo* but increasingly less so as hydrodynamic effects become more important in more viscous media.

smaller then the distance of closest approach D; for general forces, the required A may be arbitrarily small [42, 43]. Eq. (11) then becomes

$$m^* \ddot{z} + 2\gamma m^* \dot{z} + \left[k - F'_{\mathrm{ts}}(z_0)\right][z - z_0] = F_{\mathrm{ext}}(t). \tag{12}$$

This is just the equation of a forced harmonic oscillator with an effective spring constant $k^* \stackrel{\mathrm{def}}{=} k - F'_{\mathrm{ts}}(z_0)$ and the resonant (angular) frequency is

$$\omega_0 = \sqrt{\frac{k^*}{m^*}} = \sqrt{\frac{k - F'_{\mathrm{ts}}(z_0)}{m^*}}. \tag{13}$$

The frequency shift due to the interaction between the tip and the sample is hence

$$\Delta\omega_0 = \sqrt{\frac{k}{m^*}} - \sqrt{\frac{k - F'_{\mathrm{ts}}(z_0)}{m^*}} \approx -\frac{F'_{\mathrm{ts}}(z_0)}{2k}\omega_0 \tag{14}$$

for $F'_{\mathrm{ts}}(z_0) \ll k$ [9, 36, 38]. An image taken at constant frequency shift $\Delta\omega_0$ therefore corresponds to a surface of constant force gradient F'_{ts}. In practice, however, the condition $A \ll D$ is *not* fulfilled in many DFM experiments [42, 43].

SCHWARZ *et al.* [43] suggest a different approach that approximates the true anharmonic potential by two harmonic potentials and is valid for $A \gg D$, provided the decay length λ of the tip–sample interaction is much smaller than A. In this theory, the frequency shift obeys

$$\Delta\omega_0 \propto \frac{V_{\mathrm{ts}}(D)}{\sqrt{\lambda}}, \tag{15}$$

where $V_{\mathrm{ts}}(D)$ is the tip–sample interaction potential at the point of closest approach and λ the range of the interaction. It can be understood intuitively that the potential at the point of closest approach dominates the effect: The tip has its lowest speed there and experiences the potential for a longer time; since $\lambda \ll A$, the interaction is negligible at the other turning point [12, 43].

To arrive at a more accurate understanding of the tip dynamics, comparison with simulations from a realistic model of the tip–sample interaction is required and the behaviour of the feedback system determining F_{ext} has to be taken into account.

4.5.3 Amplitude Modulation

In amplitude modulation AFM (AM-AFM), the cantilever is excited at a constant frequency. The detection mechanism is used to measure the change in the amplitude response caused by the shift in the resonant frequency due to the interaction of the tip with the sample. The amplitude is either recorded directly or kept constant using a feedback loop [9, 40, 41, 43]. In this mode, further spectroscopic information may be obtained by measuring the phase shift between the excitation signal and the cantilever vibration [40].

4.5.4 Frequency Modulation

The alternative approach is frequency modulation AFM (FM-AFM), which uses a second, faster feedback loop to keep the measured amplitude constant by varying the excitation frequency and amplitude. This way, the shift in the resonance frequency can be measured directly; the excitation amplitude contains information about energy transfer to the sample [40, 41, 43, 44]. FM-AFM is preferable to AM-AFM under high vacuum conditions, because the absence of a damping medium implies a very high quality factor and the oscillation amplitude responds slowly to a change in the resonant frequency [44].

4.5.5 Dynamic Force Microscopy in a Liquid

DFM in a liquid is interesting because it is required to observe many biological samples and potentially allows atomic resolution. Modelling the dynamics is more involved, because the movement of the liquid between the cantilever and the sample becomes important and the probe can no longer be approximated by a mass on a spring [40, 45]. Compared to the same cantilever in air or vacuum, there are more and broader resonances at lower frequencies [40] and the quality factor decreases by two orders of magnitude. The latter problem can be overcome by using a positive feedback loop to drive the oscillation [46].

4.6 True Atomic Resolution

Like the STM, the AFM can in principle achieve atomic resolution [13, 38, 43, 45]. In practice, this goal is considerably harder to achieve, since important contributions to the tip–sample interaction decay slowly. However, only short-range chemical forces can be used for imaging at the atomic scale. Sharp tips are necessary to reduce the contribution of the van der Waals force [38]. In air, the meniscus force dominates the interaction; measurements must hence be taken in a liquid [45,47] or in UHV [38, 43]. While the repulsive forces used in contact AFM are short range and images with correct atomic spacings have been obtained this way, the forces on typical tips in contact mode are too large to be supported by a single microtip, preventing true atomic resolution [38, 43]. Additionally, the atomically clean surfaces of many tips and samples can stick together under UHV conditions by forming chemical bonds [38]. Atomic resolution images in UHV have only been obtained by large amplitude DFM, which prevents sticking and jump-to-contact. As with the STM, atomic resolution imaging of many materials may call for elaborate sample preparation, which can in itself require working in UHV.

4.7 Contact, Non-Contact, and Tapping Mode

In the literature the operating mode of a force microscope is often characterized as contact, non-contact (NCM), or tapping mode. In contact mode the repulsive part of the surface potential is probed. This is the usual situation for static force measurements, for which the main feedback loop is set up to increase the tip-sample distance when the detected force increases. Non-contact mode refers to operation in the attractive part of the potential. This regime is usually associated with dynamic force microscopy, which allows for increased sensitivity in detecting small attractive forces and prevents jump-to-contact. Finally, tapping mode designates a DFM experiment in which the tip samples the attractive part of the potential for most of its oscillation cycle but penetrates into the repulsive part on closest approach to the sample. In practice distinguishing between non-contact and tapping modes in DFM experiments may be difficult and requires a detailed understanding of the tip-sample interaction. FM-AFM is often identified with NCM and AM-AFM with tapping mode [40, 41]; this usage frequently, but by no means necessarily agrees with the straightforward definitions given here.

4.8 Artefacts in Atomic Force Microscope Images

4.8.1 Finite Tip Size

As shown in Fig. 4(b), real AFM tips have a finite radius of curvature r and angle α. When scanning sample features with high aspect ratios, the point of contact is not always at the apex of the tip. Consequently, such structures cannot be traced accurately. This effect is illustrated in Fig. 7: The lateral size of small features is overestimated, while the tip cannot reach the bottom of deep holes or trenches. Vertical sidewalls are imaged with rounded or slanted profiles, depending on the shape of the tip at the scale of the feature. Artefacts due to finite tip size can usually be distinguished from sample features by the fact that they do not change their orientation when the sample is rotated relative to the tip. They often appear as the repetition of a pattern that corresponds to the shape of the tip apex.

If the surface of the sample is given by $S(x, y)$ and the surface of the tip by $T(x, y)$, the image or apparent sample surface is

$$S'(x, y) = -\min_{\xi,\eta\in\mathbb{Z}} \left[T(\xi - x, \eta - y) - S(\xi, \eta) \right]. \tag{16}$$

At each point (x, y), the minimal distance between the entire shifted tip $T(\xi - x, \eta - y)$ and the entire sample surface $S(\xi, \eta)$ determines the distance by which the tip can be lowered towards the sample before contact is established.

For a known tip shape and surface Eq. (16) allows a straightforward numerical simulation of the expected image. VILLARRUBIA [48] has developed a formulation in terms of mathematical morphology and used it to show that the operation can be reversed: Given the shape of the tip and the image, the sample surface can be recovered. The reconstruction is exact where the surface has been in

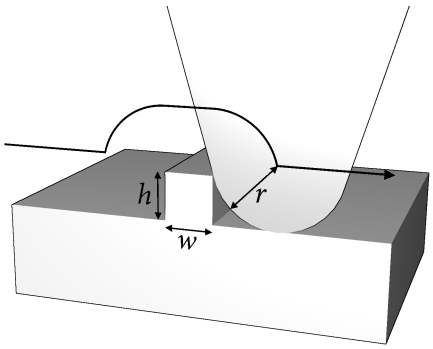

(a) Measurement using a tip with finite radius r

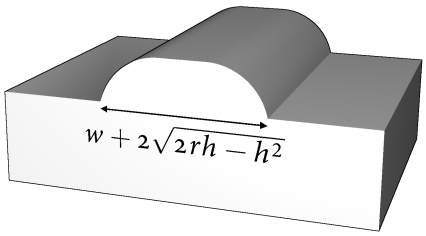

(b) Apparent topography measured in (a)

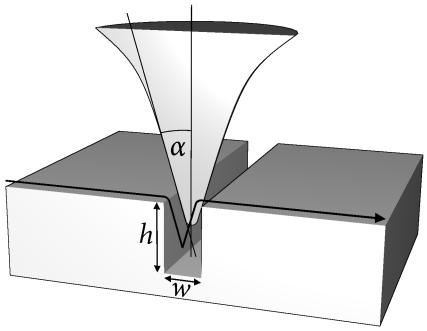

(c) Measurement using a tip with finite angle α

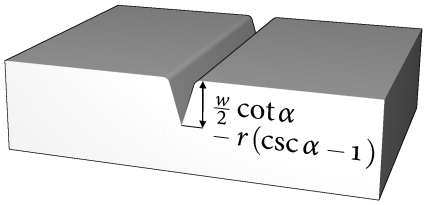

(d) Apparent topography measured in (c)

Figure 7: Finite tip size effects in an AFM measurement. Arrows indicate the trajectory of the centre of curvature of the tip.

contact with the tip and provides an upper bound elsewhere. Similarly, the tip can be reconstructed by the same method if the sample geometry is known.

In practice, the reconstruction of images is hampered by the fact that the shape of the tip apex is usually not well defined, as it can change during operation—even if care is taken to assess the specific probe by imaging a characterizer or by other means. If the tip is known to be sufficiently sharp that its area of interaction with the sample is much smaller than a given image, this image can be used to estimate the current shape of the tip via a self-consistent iterative 'blind reconstruction' method [48].

For the idealized finite size tip shown in Fig. 4(b) and surface features with simple geometries, closed expressions for the imaging error can be obtained in many cases by a simple geometrical construction; such expressions can be useful in the quick assessment of AFM images. A mesa with a rectangular cross-section of width w and height h, when imaged using a tip of finite radius of curvature $r \geq h$—Fig. 7(a) and (b)—produces an image with apparent width

$$w' = w + 2\sqrt{2rh - h^2}. \tag{17}$$

If a hole or groove is imaged with a tip that cannot reach its bottom as in Fig. 7(c) and (d), the apparent depth of the feature is given by

$$h' = \frac{w}{2}\cot\alpha \tag{18}$$

for a tip with a sharp point. If a finite radius of curvature $r \lesssim h$ is taken into account, the length

of the tip is reduced, and Eq. (18) becomes

$$h' = \frac{w}{2}\cot\alpha - r(\csc\alpha - 1). \tag{19}$$

4.8.2 Other Effects

AFMs are naturally susceptible to artefacts affecting all SPMs, such as scanner nonlinearity, smoothing and overshoot due to the finite response time of the feedback loop, and narrow-band noise mimicking a periodic surface structure. Specifically in an AFM, the tip can momentarily stick to the surface and then jump off, resulting in a spike in the image that does not correspond to a sample feature. In a DFM, for some operating parameters there can be two stable oscillation states corresponding to a single value of the tip–sample force [40]. In this case, the apparent topography can jump between two levels with an approximately constant offset between them. The jumps are usually random, but can sometimes mimic a step in the sample.

5 Scanning-Probe-Based Lithography

5.1 Manipulation of Individual Atoms

A famous example of the ability of the SPM to shape matter at an atomic scale is the 'quantum corral' of iron atoms on a copper surface created by Crommie *et al.* [49] via the controlled movement of adatoms using an STM. The sensitivity of the STM to the local electronic density of states has been used to image the standing wave corresponding to an electron trapped in the artificial enclosure.

In order to manipulate individual atoms, the STM must operate under UHV, which is required for atomic resolution imaging. Performing the experiment at liquid helium temperatures improves the stability and may be necessary to prevent diffusion of the adatoms. The tip can be used to move individual atoms either in a parallel process, in which the connection to the surface is never broken, or in a perpendicular process, in which the atom detaches from the surface and is adsorbed at the tip. In the parallel process, the electric field at the apex of the tip can be increased to enhance diffusion in the desired direction. Alternatively, the tip can be lowered towards an adatom by changing the feedback parameter until the chemical forces allow for sliding the atom across the surface. The perpendicular process transfers atoms between the surface and the tip by approaching and retracting the probe or by applying a voltage pulse to overcome the potential barrier [50].

5.2 Nanoindentation

AFMs can also be used to modify a sample mechanically. The tip is pressed against the workpiece with a force exceeding the threshold for inelastic deformation and indents or chips the surface. It must be attached to a sufficiently stiff cantilever to support the interaction force and commonly consists of a hard material, *e.g.*, diamond, to minimize wear. Apart from the sharpness and durability of the tip, the performance of this method depends critically on the mechanical properties of the sample itself; under optimal conditions, a resolution of 10 nm can be realized [51, 52]. Since high resolution modifications can only be achieved with certain substrates, a separate surface layer consisting of a soft polymer, metal, or oxide is sometimes applied and the pattern transferred using an auxiliary etch technique. Nanoscratching with an oscillating force as in a DFM helps avoid sticking of the tip [51, 53, 54].

5.3 Electrical and Optical Surface Modification

A voltage pulse applied to a conducting STM or AFM tip can modify the substrate in various other ways. Field emission from an STM tip can be used to expose organic resists at length scales comparable with the best electron beam writers. Joule heating due to local high current densities and field-assisted evaporation have been proposed as mechanisms for the surface modification observed in some experiments. The electrical field in the vicinity of an STM or AFM tip can activate the chemical vapour deposition (CVD) of some materials, especially metals. Finally, the voltage difference can be used to locally enable electrochemical processes [52].

A special case of the latter technique is the local

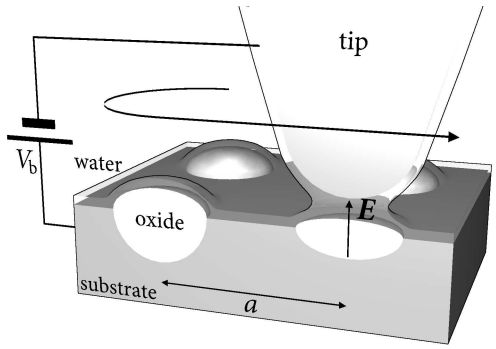

Figure 8: Local anodic oxidation

anodic oxidation of metal or semiconductor surfaces, which is illustrated in Fig. 8. It requires that the instrument operate in air under ambient conditions, so that oxide-passivated hydrophilic surfaces will be covered by a thin layer of adsorbed water [55]. After the initial oxide layer has been created, further oxidation requires the migration of oxyanions, substrate cations, or both through the oxide film. The electric field set up in the oxide by the voltage difference between the probe and the substrate enhances their diffusion into the surface. If an SPM probe is brought close to the surface and a bias is applied to it, a water meniscus, which acts as a source of oxygen anions, forms between the tip and the sample [56–58]. As the formation of this meniscus is essential for successful anodization, the technique depends on the ambient humidity, which affects the thickness and continuity of the adsorbed water layer.

Similar to the situation with nanoindentation, these methods critically depend on the chemical and electrical properties of the involved materials; sometimes an additional pattern transfer process can circumvent this limitation. Optical techniques include the exposure of conventional photoresist and other photoactive surfaces by illumination mode NFSOM.

6 Summary

The SPM is a versatile tool that can measure and manipulate a surface at length scales from fractions of an Ångström up to several microns. The concept can be used with a large range of different tip–sample interactions, and many different physical properties of the sample can be mapped. Advances in scanner and noise control technology mean that the fundamental limit to the resolution of an SPM method is determined by the size and shape of the probe and the range of the interaction it uses. Correct interpretation of images requires a detailed understandig of this interaction at the relevant scale.

References

[1] T. O. Stadelmann. *Antidot Superlattices in InAs–GaSb Double Heterostructures: Transport Studies*. DPhil thesis, University College, University of Oxford, 2006.

[2] E. T. Yu. Nanoscale characterization of semiconductor materials and devices using scanning probe techniques. *Materials Science and Engineering*, R17:147–206, 1996.

[3] G. Schmalz. Über Glätte und Ebenheit as physikalisches und physiologisches Problem. *Zeitschrift des Verbandes Deutscher Ingenieure*, 73:144–161, October 1929.

[4] R. Young, J. Ward, and F. Scire. Observation of metal-vacuum-metal tunneling, field emission, and the transition region. *Physical Review Letters*, 27(14):922–924, October 1971.

[5] R. Young, J. Ward, and F. Scire. The topographiner: An instrument for measuring surface microtopography. *Review of Scientific Instruments*, 43(7):999–1011, July 1972.

[6] G. Binnig and H. Rohrer. Scanning tunneling microscopy—from birth to adolescence. *Reviews of Modern Physics*, 59(3):615–625, July 1987. Nobel Lecture.

[7] G. Binnig, H. Rohrer, C. Gerber, and E. Weibel. Surface studies by scanning tunneling microscopy. *Physical Review Letters*, 49(1):57–61, July 1982.

[8] G. Binnig, C. F. Quate, and C. Gerber. Atomic force microscope. *Physical Review Letters*, 56(9):930–933, March 1986.

[9] Y. Martin, C. C. Williams, and H. K. Wickramasinghe. Atomic force microscope-force mapping and profiling on a sub-100 Å scale. *Journal of Applied Physics*, 61(10):4723–4729, May 1987.

[10] U. Dürig, D. W. Pohl, and F. Rohner. Near-field optical-scanning microscopy. *Journal of Applied Physics*, 59(10):3318–3327, May 1986.

[11] R. C. Reddick, R. J. Warmack, and T. L. Ferrell. New form of scanning optical microscopy. *Physical Review A*, 39(1):767–770, January 1989.

[12] D. Drakova. Theoretical modelling of scanning tunnelling microscopy, scanning tunnelling spectroscopy and atomic force microscopy. *Reports on Progress in Physics*, 64:205–290, 2001.

[13] W. A. Hofer, A. S. Foster, and A. L. Shluger. Theories of scanning probe microscopes at the atomic scale. *Reviews of Modern Physics*, 75:1287–1331, October 2003.

[14] S. Gasiorowicz. *Quantum Physics*, chapter 5. John Wiley & Sons, New York, second edition, 1996.

[15] J. Tersoff and D. R. Hamann. Theory and application for the scanning tunneling microscope. *Physical Review Letters*, 50(25):1998–2001, June 1993.

[16] J. G. Simmons. Generalized formula for the electric tunnel effect between similar electrodes separated by a thin insulating film. *Journal of Applied Physics*, 34(6):1793–1803, June 1963.

[17] C. Girard, C. Joachim, and S. Gauthier. The physics of the near-field. *Reports on Progress in Physics*, 63:893–938, 2000. read 19th July 2005; C.

[18] J. W. P. Hsu. Near-field scanning optical microscopy studies of electronic and photonic materials and devices. *Materials Science and Engineering*, 33:1–50, 2001.

[19] L. E. Cross. Ferroelectric materials for electromechanical transducer applications. *Materials Chemistry and Physics*, 43:108–115, 1996.

[20] L. Libioulle, A. Ronda, M. Taborelli, and J. M. Gilles. Deformations and nonlinearity in scanning tunneling microscope images. *Journal of Vacuum Science and Technology B*, 9(2):655–658, March/April 1991.

[21] K. R. Koops, P. M. L. O. Scholte, and W. L. de Koning. Observation of zero creep in piezoelectric actuators. *Applied Physics A*, 68:691–697, 1999.

[22] K. Dirscherl, J. Garnæs, and L. Nielsen. Modeling the hysteresis of a scanning probe microscope. *Journal of Vacuum Science and Technology B*, 18(2), 621–625 2000.

[23] H.-C. Yeh, W.-T. Ni, and S.-S. Pan. Digital closed-loop nanopositioning using rectilinear flexure stage and laser interferometry. *Control Engineering Practice*, 13:559–566, 2005.

[24] J. E. Griffith, G. L. Miller, C. A. Green, D. A. Grigg, and P. E. Russell. A scanning tunneling microscope with a capacitance-based position monitor. *Journal of Vacuum Science and Technology B*, 8(6):2023–2027, November/December 1990.

[25] B. Cappella and G. Dietler. Force-distance curves by atomic force microscopy. *Surface Science Reports*, 34:1–104, 1999.

[26] H.-C. Zhang, A. Sasaki, J. Fukaya, and H. Aoyama. Surface roughness observation by scanning tunneling microscopy using a monolithic parallel spring. *Journal of Vacuum Science and Technology B*, 12(3):1669–1672, May/June 1994.

[27] G. Binnig and D. P. E. Smith. Single-tube three-dimensional scanner for scanning tunneling microscopy. *Review of Scientific Instruments*, 57(8):1688–1689, March 1986.

[28] A. Franks. Nanotechnology. *Journal of Physical Engineering: Scientific Instruments*, 20:1442–1451, 1987.

[29] T. Mariani, C. Frediani, and C. Ascoli. Non-conventional, inexpensive 3-D scanners for probe microscopy. *Applied Physics A*, 66:S35–S40, 1998.

[30] A. Lewis and K. Lieberman. Flat scanning stage for scanned probe microscopy. US Patent 5,705,878, January 1998.

[31] F. E. Scire. Planar biaxial micropositioning stage. US Patent 4,506,154, March 1985.

[32] T. Mariani, C. Frediani, and C. Ascoli. A three-dimensional scanner for probe microscopy on the millimetre scale. *Applied Physics A*, 66:S861–S866, 1998.

[33] G. K. Binnig, W. Haeberle, H. Rohrer, and D. P. E. Smith. Fine positioning apparatus with atomic resolution. US Patent 5,808,302, September 1998.

[34] H. Rothuizen, U. Drechsler, G. Genolet, W. Häberle, M. Lutwyche, R. Stutz, R. Widmer, and P. Vettiger. Fabrication of a micromachined magnetic $X/Y/Z$ scanner for parallel scanning probe applications. *Microelectronic Engineering*, 53:509–512, 2000.

[35] J. E. Sader. Susceptibility of atomic force microscope cantilevers to lateral forces. *Review of Scientific Instruments*, 74(4):2438–2443, April 2003.

[36] R. Erlandsson, G. M. McClelland, C. M. Mate, and S. Chiang. Atomic force microscopy using optical interferometry. *Journal of Vacuum Science and Technology A*, 6(2):266–270, March/April 1988.

[37] S. Alexander, L. Hellemans, O. Marti, J. Schneir, V. Elings, P. K. Hansma, M. Longmire, and J. Gurley. An atomic-resolution atomic-force microscope implemented using an optical lever. *Journal of Applied Physics*, 65(1):164–167, January 1989.

[38] F. J. Giessibl. Atomic resolution of the silicon (111)-(7×7) surface by atomic force microscopy. *Science*, 267(5194):68–71, January 1995.

[39] T. Akiyama, S. Gautsch, N. F. de Rooij, U. Staufer, P. Niedermann, L. Howald, D. Müller, A. Tonin, H.-R. Hidber, W. T. Pike, and M. H. Hecht. Atomic force microscope for planetary applications. *Sensors and Actuators A*, 91:321–325, 2001.

[40] R. García and R. Pérez. Dynamic atomic force microscopy methods. *Surface Science Reports*, 47:197–301, 2002.

[41] G. Couturier, R. Boisgard, L. Nony, and J. P. Aimé. Non-contact atomic force microscopy: Stability criterion and dynamical responses of the shift of frequency and damping signal. *Review of Scientific Instruments*, 74(5):2726–2734, May 2003.

[42] H. Hölscher, U. D. Schwarz, and R. Wiesendanger. Calculation of the frequency shift in dynamic force microscopy. *Applied Surface Science*, 140:344–351, 1999.

[43] U. D. Schwarz, H. Hölscher, and R. Wiesendanger. Atomic resolution in scanning force microscopy: Concepts, requirements, contrast mechanisms, and image interpretation. *Physical Review B*, 62(19):13089–13097, November 2000.

[44] R. Bennewitz, M. Bammerlin, M. Guggisberg, C. Loppacher, A. Barato, E. Meyer, and H.-J. Güntherodt. Aspects of dynamic force microscopy on NaCl/Cu(111): Resolution, tip–sample interactions and cantilever oscillation characteristics. *Surface and Interface Analysis*, 27:462–466, 1999.

[45] F. M. Ohnesorge. Towards atomic resolution noncontact dynamic force microscopy in a liquid. *Surface and Interface Analysis*, 27:179–385, 1999.

[46] J. Tamayo, A. D. L. Humphris, R. J. Owen, and M. J. Miles. High-*Q* dynamic force microscopy in liquid and its application to living cells. *Biophysical Journal*, 81:526–537, July 2001.

[47] F. M. Ohnesorge and G. Binnig. True atomic resolution by atomic force microscopy through repulsive and attractive forces. *Science*, 360(5113):1451–1456, June 1993.

[48] J. S. Villarrubia. Algorithms for scanned probe microscope image simulation, surface reconstruction, and tip estimation. *Journal of Research of the National Institute of Standards and Technology*, 102(4):425–454, July/August 1997.

[49] M. F. Crommie, C. P. Lutz, and D. M. Eigler. Confinement of electrons to quantum corrals on a metal surface. *Science*, 262(5131):218–220, October 1993.

[50] J. A. Stroscio and D. M. Eigler. Atomic and molecular manipulation with the scanning tunneling microscope. *Science*, 254(5036):1319–1326, November 1991.

[51] Y. Kim and C. M. Lieber. Machining oxide thin films with an atomic force microscope: Pattern and object formation on the nanometer scale. *Science*, 257:375–377, July 1992.

[52] R. M. Nyffenegger and R. M. Penner. Nanometer-scale surface modification using the scanning probe microscope: Progress since 1991. *Chemical Reviews*, 97:1195–1230, 1997.

[53] M. Wendel, B. Irmer, J. Cortes, R. Kaiser, H. Lorenz, J. P. Kotthaus, A. Lorke, and E. Williams. Nanolithography with an atomic force microscope. *Superlattices and Microstructures*, 20(3):349–356, 1996.

[54] U. Kunze. Nanoscale devices fabricated by dynamic ploughing with an atomic force microscope. *Superlattices and Microstructures*, 31(1):3–17, 2002.

[55] J. A. Dagata, J. Schneir, H. H. Harary, C. J. Evans, M. T. Postek, and J. Bennett. Modification of hydrogen-passivated silicon by a scanning tunneling microscope operating in air. *Applied Physics Letters*, 56(20):2001–2003, May 1990.

[56] A. E. Gordon, R. T. Fayfield, D. D. Litfin, and T. K. Higman. Mechanisms of surface anodization produced by scanning probe microscopes. *Journal of Vacuum Science and Technology*, 13(6):2805–2808, November/December 1995.

[57] M. Calleja, J. Anguita, R. García, K. F. Pérez-Murano, and J. A. Dagata. Nanometre-scale oxidation of silicon surfaces by dynamic force microscopy: reproducibility, kinetics and nanofabrication. *Nanotechnology*, 10:34–38, 1998.

[58] J. A. Dagata, T. Inoue, J. Itoh, K. Matsumoto, and H. Yokoyama. Role of space charge in scanned probe oxidation. *Journal of Applied Physics*, 84(12):6891–6900, December 1998.